Bulletin of the JSME, Vol. 22, No. 172, October 1979



Paper No. 172-16

534.14:621-52

# Analysis of Vibration in Hydraulic Drive System*

By Hajime AKASHI**, Takayuki NAKAGAWA*** and Tsuyoshi OSUMI****

It is well known that stick-slip motion often occurs while operating a hydraulic drive system with plane slide-ways at low speed and there are a number of researches reported on the analysis of such a motion.

The authors made similar experiments with a hydraulic system with comparatively small friction and found that vibrations without sticking could occur as well as the stick-slip motion. A detailed analysis of such a motion was made and the result was compared with the experiment. The time dependency of the maximum static friction and also the variation of a part of the friction characteristic were taken into consideration.

The comparison shows a striking agreement between the analysis and the experiment, justifying to a considerable extent the assumptions made in the analysis, and clarifying the fundamental mechanism of such a motion in the drive system of similar structure.

## 1. Introduction

It is well known that vibrations and stick-slip motions often occur in low speed operation of hydraulic driving systems. A number of researches on these motions have been made and many reports [1]~[3] are available, e.g. by Matsuzaki et al. Most of these reports are on plane slide-ways used in the feed mechanism of machine tools. There are also reports [9] ~ [15] on the relation between the motion and the friction characteristics, load or other factors. The motions were usually analyzed by a dynamic model.

The authors made experiments on a hydraulic system similar to the ones treated in other papers, but with guide-ways having a relatively small friction.

In their experiments, various types of vibrations were observed at low speed. Especially the vibrations without sticking were clearly observed as well as the stick-slip motions. The previous studies did not provide any satisfactory, unified analysis of these motions.

The authors recorded the motions during high and low speed operations and examined the flow-pressure characteristics carefully. The analysis of the vibration was made by a set of nonlinear equations of motion and the transient motions were investigated considering the time dependency of the maximum static friction.

As the result, the influence of supply pressure, mass, volume and modulus of compressibility of hydraulic fluid on the characteristics of the motion was made clear.

The recorded pressure and velocity with respect to time coincide quite well with the same quantities obtained by calculation using the phase plane analysis.

## 2. Experiments: experimental set-up, method and results

### 2.1 Experimental set-up

Figure 1 shows a schematic diagram of the experimental set-up. Oil is fed into the hydraulic cylinder through a flow control valve or a servo-valve by an oil supply device and the load is moved by a hydraulic piston. The load is a sliding table with weight on it and the table is supported by the steel balls placed in V-type gutters. The pressure difference $P$ between $P_1$ and $P_2$, the pressures at the ends of the pipes, and the velocity of the piston $V$, are recorded on an X-Y recorder and a pen recorder. The velocity is obtained by electrically differentiating the voltage signal indicating the position of the piston. The accuracy of the measurement was checked by calibration, [16] and it was high enough between 0.05cm/sec and 3cm/sec,

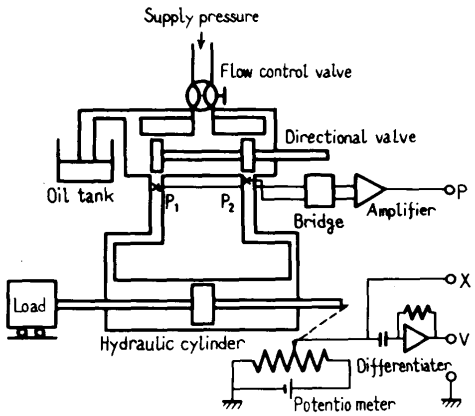


Fig.1 Schematic diagram of the apparatus

* Received 10th October, 1976.

** Professor, Faculty of Engineering, Kyoto University.

*** Assistant Professor, Faculty of Engineering, Toyama University.

**** Research Assistant, Faculty of Engineering, Toyama University.

which is the velocity measured in this experiment. The pressure is picked up by semi-conductor strain gages.

2.2 Measurement and results

In order to obtain the characteristics of the total friction in the system, the piston is driven at various constant speeds by controlling the opening of the flow control valve. By plotting the pressure $P$ against the speed $V$ for various anounts of load, the friction characteristics of the system are obtained. In this measurement a servo-valve is used to suppress the vibratory motion of the piston, which tends to occur at low piston velocity. Although it is not possible to suppress the vibration entirely, it is helpful to confine this motion to a small driving velocity for the determination of friction characteristics.

Figure 2 shows an example of the records of pressure difference $P$ against the velocity $V$, obtained by setting the electric current $I$ of servo-valve at various values. The supply pressure $P_S$ (5kg/cm$^2$-10kg/cm$^2$) and the load $W$ (20kg-100kg) are other parameters. The points indicated at $I$=2mA and 3mA, are not actually stable but vibratory points. The piston at these points and the points in between, makes a vibratory motion and hence does not give exact points on the friction characteristic. This portion of the friction characteristic has to be estimated from the rest of the characteristic curve. The friction characteristic obtained in this way is shown in Fig.3 for various quantities of load. The dotted line shows a portion where the characteristic was estimated from the rest of the curve.

One outstanding feature of the obtained friction characteristics is that it has a portion of positive gradient near zero velocity in the $V$-$P$ plane. This is confirmed by driving the piston at very low speed of less than 0.006cm/sec. This portion of the friction is too small to be shown in Fig.3, and is shown separately in Fig.4.

Replacing the servo-valve by an ordinary manual flow control valve, it is found that the vibration occurs in a considerably larger range of piston velocities. The pressure and velocity changes during the vibratory motion were recorded by the pen recorder for various parameters. Two examples of such recordings are shown in Fig.5.

Some vibration records on the $V$-$P$ plane and the points of stable piston motion are shown together in Fig.6. In the figure, points $A$, $B$, $C$ and $D$ are singular points. Among these, $A$ and $B$ are estimated points on the friction curve, $C$ and $D$ being the stable points which correspond to smooth movements of the piston.

From the records of pressure against time during stick-slip motions, the maximum static friction was measured after each sticking. By plotting on the $P$-$t$ plane the pressure at which the piston starts to slip after each sticking, a curve of "Maximum static friction" shown by $A$-$D$-$B$ was obtained as in Fig.7. After the piston comes to a stop during a stick-slip motion, say at $P'_C$ in Fig.7, the pressure builds up along the chain line $C'D'$, until at $D'$ it reaches the point corresponding to the maximum static force and the piston starts to slip. It is obvious that the maximum static friction is an increasing function of the time interval in which

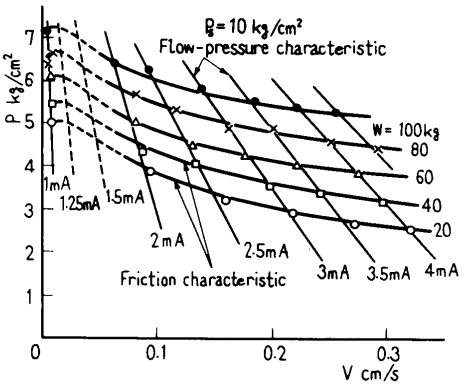


Fig.3 Friction and flow-pressure characteristics in $V$-$P$ plane

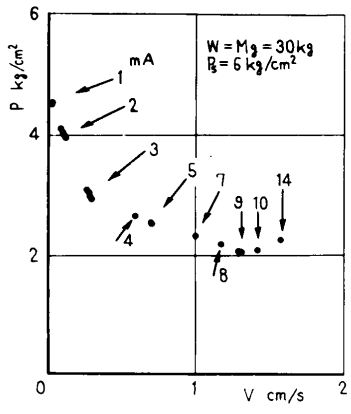


Fig.2 Stationary points in $V$-$P$ plane (Parameter: electric current in servo-valve)

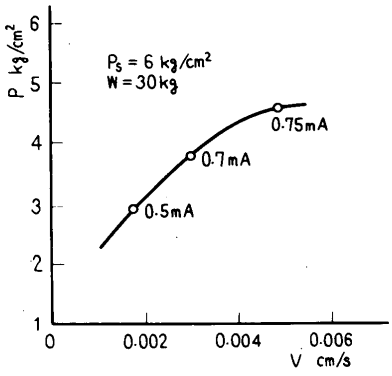


Fig.4 Stationary point in $V$-$P$ plane ($V$ in the neighborhood of zero)

the piston stays still. Turning back to the $V$-$P$ plane of Fig.6, the starting point of the limit cycle for this stick-slip motion should correspond to the maximum static friction of $D'$. The friction characteristic during such a vibration should be considered variable in the region near zero velocity. This situation will be discussed again later in section 4.1.

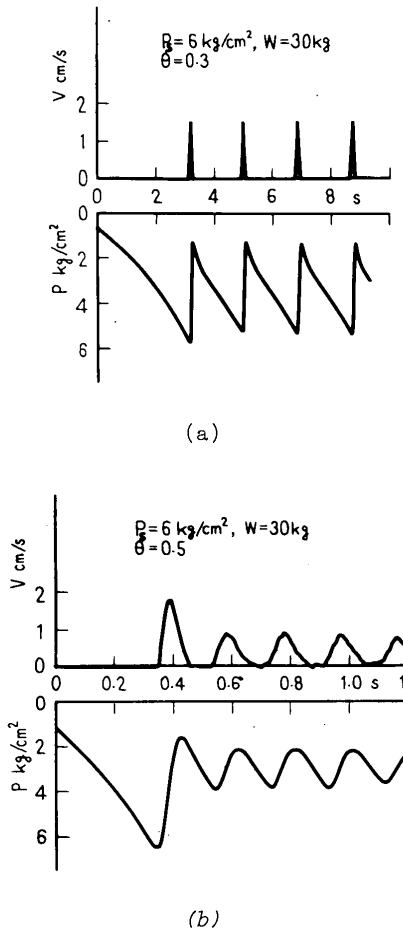


Fig.5 Experimental wave forms of $V$ and $P$

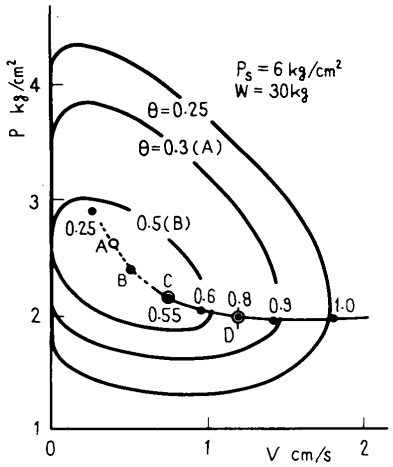


Fig.6 Limit cycles and the corresponding singular points; and stable equilibrium points

## 3. Analysis of the motion of the piston

### 3.1 Equation of motion

For simplicity, the hydraulic driving system in Fig.1 is replaced by a schematic diagram shown in Fig.8. In the following are shown the notations of various quantities used in the analysis.

$A$, $A_c$ : Areas of the effective cross section of the piston and cross section of the pipe. $cm^2$

$B$ : Width of the port of the flow control valve. cm

$C_1$, $C_2$ : Constants

$F$ : Coefficient of friction

$f(dX/dt)$ : Friction as a function of the velocity

$G$ : Volume of the oil contained in one side of the cylinder and the pipe $cm^3$

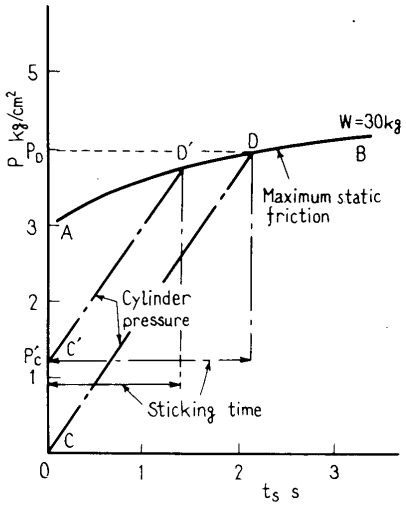


Fig.7 Relation between maximum static friction, sticking time and cylinder pressure

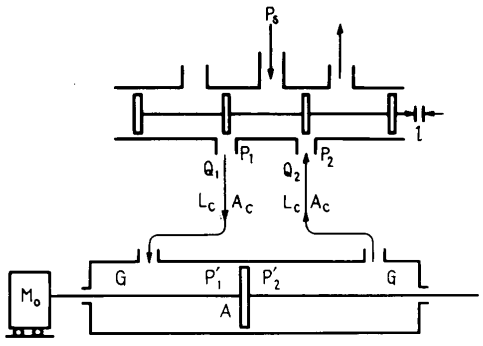


Fig.8 Schematic diagram of hydraulic driving system

$g$ : Gravitational conversion constant cm/s$^2$
$H_1(P), H_2(V)$: Functions of pressure and velocity
$L$, $L_C$ : Half the stroke of piston and length of conduit cm
$l$ : Displacement of the spool valve cm
$M_0$, $M_e$ : Mass of the load and effective mass of oil $M_0 + M_e = M$ kgs$^2$/cm
$m$ : Magnifying ratio of velocity axis kgs/cm$^3$
$P_1$, $P_2$ : Pressures at the ends of pipes at the valve kg/cm$^2$
$P_1'$, $P_2'$ : Pressures at left and right sides of the piston kg/cm$^2$
$P_S$, $p$ : Supply pressure and deviation of the pressure kg/cm$^2$
$Q_1$, $Q_2$ : Flow volumes in left and right hand side pipes cm$^3$/s
$S$, $S_0$ : Orifice area of the valve and the total orifice area of valve $S = Bl$, $S_0 = Bl_0$ cm$^2$
$t$, $t_S$ : Time and sticking time sec
$V$, $V_1$ : Piston velocity cm/s
$V_1 = mV$ kg/cm$^2$
$X$ : Displacement of the piston ( positive for movement toward right) cm
$\alpha(\theta)$, $\theta$: Flow coefficient and ratio of opening of the valve : $\theta = S/S_0$
$\beta$ : Modulus of compressibility of oil cm$^2$/kg
$\gamma$ : Specific gravity of oil kg/cm$^3$
$\nu$ : Kinematic viscosity cm$^2$/s
$\rho$ : Constant
$\phi, \phi'$ : Displacement angles

When the piston moves toward right, the following equations hold for $Q_1$ and $Q_2$

$$Q_1 = C_1\frac{dX}{dt} + C_2\frac{dP_1}{dt} \quad \cdots\cdots(1)$$

$$Q_2 = C_1\frac{dX}{dt} - C_2\frac{dP_2}{dt} \quad \cdots\cdots(2)$$

If the piston moves at a constant speed, $dV/dt$ and $dP/dt$ are equal to zero. Accordingly

$$Q_1 = Q_2 = C_1\frac{dX}{dt} = A\frac{dX}{dt} \quad \cdots\cdots(3)$$

In other words, as $C_1$ is equal to the effective area of the piston, $C_1 = A$.

If the oil flows but the piston does not move, $dX/dt$ is equal to zero, and so

$$Q_1 = C_2\frac{dP_1}{dt} = \beta G\frac{dP_1}{dt} \quad \cdots\cdots(4)$$

and

$$Q_2 = -C_2\frac{dP_2}{dt} = -\beta G\frac{dP_2}{dt} \quad \cdots\cdots(5)$$

Here $G$ for the pipe in the right hand side is equal to $G$ for the pipe in the left hand side. In other words, the piston is assumed to be located at the center of the cylinder. Therefore we may put $C_2 = \beta G$. If we add Eq.(1) to Eq.(2), and put $C_1 = A$ and $C_2 = \beta G$, then we have

$$Q_1 + Q_2 = 2A\frac{dX}{dt} + \beta G\frac{d(P_1 - P_2)}{dt} \quad \cdots(6)$$

$Q_1$ and $Q_2$ can be written as follows in terms of the pressures and the open ratio of opening of the valve.

$$Q_1 = \alpha(\theta)\sqrt{P_S - P_1} \quad \cdots\cdots(7)$$

$$Q_2 = \alpha(\theta)\sqrt{P_2} \quad \cdots\cdots(8)$$

The pressure of the outlet side of the valve can be assumed to be atmospheric pressure. Thus

$$Q_1 + Q_2 = \alpha(\theta)\{\sqrt{P_S - P_1} + \sqrt{P_2}\} \quad \cdots(9)$$

is obtained. The right hand side of Eq.(9) is a nonlinear function of $P_1$ and $P_2$. This is approximated[17] as the first order function of $P = P_1 - P_2$ as follows.

$$Q_1 + Q_2 \fallingdotseq \alpha(\theta)\sqrt{P_S}\left(\rho - \frac{P}{P_S}\right) \quad \cdots\cdots(10)$$

Here, $\rho$ takes such value that the approximate equation (10) is nearly equal to Eq.(9) in all the range of the movement. Usually it is a value between 1 and 1.5.[17] From Eq.(6) and Eq.(10), the following flow-pressure equation is obtained.

$$2A\frac{dX}{dt} + \beta G\frac{dP}{dt} = \alpha(\theta)\sqrt{P_S}\left(\rho - \frac{P}{P_S}\right) \quad (11)$$

Now, the equation of motion of the load of the system is given as follows.

$$M_0\frac{d^2X}{dt^2} + f\left(\frac{dX}{dt}\right) = A(P_1' - P_2') \quad \cdots\cdots(12)$$

Here, $f(dX/dt)$ is a friction curve obtained from the experiment and is generally nonlinear. It is known that the pressure differences, $P_1 - P_1'$ and $P_2' - P_2$, are given as the sum of the friction loss due to oil viscosity and the loss due to the inertia of the mass, and are indicated as follows, where the length of inlet pipe is assumed to be equal to the outlet pipe, $L_C$.

$$P_1 - P_1' = P_2' - P_2 = \frac{8\pi\nu\gamma L_C}{A_C^2 g}A\frac{dX}{dt} + \frac{1}{A_C^2}\left(\frac{\gamma L_C A_C}{g}\right)A\frac{d^2X}{dt^2} \quad \cdots\cdots(13)$$

From this equation,

$$P_1 - P_2 = P_1' - P_2' + \frac{16\pi\nu\gamma L_C}{A_C^2 g}A\frac{dX}{dt} + \frac{2}{A_C^2}\left(\frac{\gamma L_C A_C}{g}\right)A\frac{d^2X}{dt^2} \quad \cdots\cdots(14)$$

From Eq.(14) and Eq.(12), putting $P = P_1 - P_2$,

$$(M_0 + M_e)\frac{d^2X}{dt^2} + f\left(\frac{dX}{dt}\right) + F\frac{dX}{dt} = AP \quad \cdots\cdots(15)$$

where $M_e = \frac{2A^2}{A_C^2}\left(\frac{\gamma L_C A_C}{g}\right)$, $F = \frac{16\pi\nu\gamma L_C A^2}{A_C^2 g}$

$M_e$ is a modified term of the mass of the load considering the inertia of the oil, and $F(dX/dt)$ is a revised term of friction force considering the friction in the pipe. By solving the simultaneous equations of (11) and (15), the motion of the system can be obtained.

3.2 Graphical method of solution

Since the equation of motion is nonlinear, a graphical method [18][19] will be used to solve it for the trajectory in the phase plane of $P$ and $V$.

writing

$$\frac{dX}{dt} = V \quad \cdots\cdots(16)$$

We have

$$\frac{dP}{dt} = \frac{1}{\beta G}\{\alpha(\theta)\rho\sqrt{P_S} - \frac{\alpha(\theta)}{\sqrt{P_S}}P - 2AV\} \quad \cdots\cdots(17)$$

From Eq.(15),

$$\frac{dV}{dt} = \frac{1}{M_0 + M_e}\{AP - f(V) - FV\} \cdots(18)$$

Eliminating $t$ from these equations,

$$\frac{dP}{dV} = -\frac{M}{\beta G}\frac{(\frac{\alpha(\theta)}{\sqrt{P_S}}P + 2AV - \alpha(\theta)\rho\sqrt{P_S})}{AP - \{FV + f(V)\}}$$

$$= -\frac{2M}{\beta G}\frac{V + \frac{\alpha(\theta)}{2A\sqrt{P_S}}P - \frac{\alpha(\theta)\rho}{2A}\sqrt{P_S}}{P - \frac{1}{A}\{FV + f(V)\}} \quad \cdots\cdots(19)$$

where $M = M_0 + M_e$

Unless $2M/\beta G$ is equal to unity in the above, it is not possible to apply Li'enard's graphical method [18][19] to Eq. (19). We therefore transform the variable $V$ to $V_1$ and obtain the equivalent equation to Eq.(19) as follows.

$$V = V_1/m, \quad m = \sqrt{2M/\beta G}$$

$$\frac{dP}{dV_1} = -\frac{V_1 + H_1(P)}{P - H_2(V_1)} \quad \cdots\cdots(20)$$

where

$$H_1(P) = \frac{m\alpha(\theta)}{2A\sqrt{P_S}}P - \frac{m\alpha(\theta)\rho}{2A}\sqrt{P_S} \quad \cdots(21)$$

$$H_2(V_1) = \frac{F}{mA}V_1 + \frac{1}{A}f(\frac{V_1}{m}) \quad \cdots\cdots(22)$$

Now it is possible to apply Li'enard's method to Eq.(20). The procedure of obtaining the gradient of the trajectory at any given point is illustrated in Fig.9. First, draw the curves of the following equations on the phase plane.

$$V_1 = -H_1(P) \quad \cdots\cdots(23)$$

$$P = H_2(V) \quad \cdots\cdots(24)$$

To obtain the gradient at a given point $A_1$, draw a rectangle as shown by the dotted line, with the apexes $B_1$ and $C_1$ on the above curves. Then the gradient is given by $\overline{A_1A_2}$, perpendicular to the diagonal $\overline{D_1A_1}$. This simple method is applied to points near $A_1$, say $A_2$ and the approximate trajectory of Eq.(20) is obtained. That this procedure gives the solution is seen as follows. Let $\phi'$ be the angle as shown in Fig.9, then

$$\tan\phi' = (\frac{dP}{dV_1})_{A_1} = \tan_L C_1A_1D_1 = -\frac{C_1D_1}{C_1A_1}$$

$$= -\frac{V_{11} + H_1(P)}{P - H_2(V_{11})} \quad \cdots\cdots(25)$$

Let $\phi$ be the angle as shown in the figure, then

$$\tan\phi = \frac{A_1C_1}{C_1D_1} = \frac{P - H_2(V_{11})}{V_{11} + H_1(P)} \cdots(26)$$

We see $\tan\phi \cdot \tan\phi' = -1$, which proves that this graphical procedure gives a correct gradient.

The trajectory obtained in this way in the $V_1$-$P$ plane is transferred to the $V$-$P$ plane by contracting or stretching the abscissa by a factor of $m$. Figs.10 and 11 show examples of the trajectories obtained by this graphical method (the right half plane), considering also the time dependency of the maximum static friction ( the left half plane). Starting from zero pressure, the trajectory passes through a short transient state and then moves into the limit cycle. The time sequence of the motion is indicated by the numbers in circles.

The limit cycle in Fig.10 represents a stick-slip motion and the time interval of the stuck state is found from the left half plane. The example in Fig.11 also settles into a limit cycle but without sticking portion, although in the transition the piston sticks for a short period. (from ④ to ⑤ = ⑥ )

In the left half plane of Fig.10, for example, the line from ① to ② indicates the way the pressure is built up while the piston is stationary. This curve can be calculated by Eq.(11) setting $dX/dt = 0$ since $X$ does not vary in this period. The following equation represents the curve of the cylinder pressure rise with time.

$$P = \rho P_S\left[1 - \exp\{-\frac{\alpha(\theta)t}{\beta G\sqrt{P_S}}\}\right]$$

$$+ P_0\exp\{-\frac{\alpha(\theta)t}{\beta G\sqrt{P_S}}\} \quad \cdots\cdots(27)$$

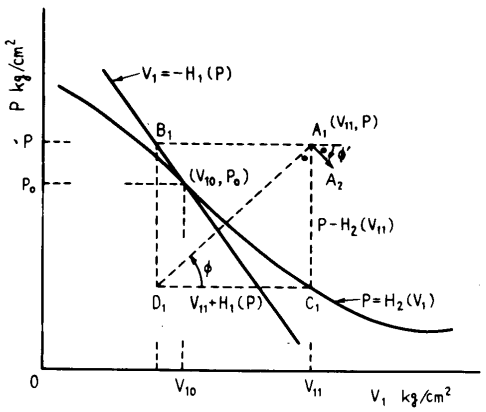


Fig.9 Procedures of graphical method

3.3 Wave form of the vibration in the

variables $P$ and $V$

It is possible to obtain the wave form from the trajectory in the $V$-$P$ plane. For this we approximate the deviations of $P$ and $V$ by the ratio of the increments of these variables and the time increment. We have then

$$\frac{\Delta P}{\Delta t} = \frac{1}{\beta G}\left\{\alpha(\theta)\sqrt{P_s}\left(\rho - \frac{P}{P_s}\right) - 2AV\right\} \quad \cdots\cdots\cdots\cdots(28)$$

and

$$\frac{\Delta V}{\Delta t} = \frac{1}{M}\left\{AP - f(V) - FV\right\} \quad \cdots\cdots\cdots(29)$$

By choosing $\Delta t$ reasonably small and calculating $\Delta P$ or $\Delta V$ by Eq.(28) or (29) respectively, we may construct an approximate wave form of the pressure and velocity during the vibration. Fig.12(a) shows the result of such a procedure for the case of stick-slip motion for both $P$ and $V$. The dotted lines represent the measurement of the actual motion of the piston for the corresponding conditions. Fig.12(b) shows similarly the result of the construction of the wave form by Eqs.(28) and (29), using the graphical solution of Fig. 11. The dotted line shows the result of experiment under the same condition. It is seen that the two sets of curves agree strikingly well considering the approximation inherent in the graphical method.

3.4 Stability analysis

The condition of the vibratory motion of the piston in this system is found by applying the theory of stability for nonlinear systems. Some motion of this system will be checked if the conditions of the motions satisfy the stability criterion.

Going back to Eq.(19), the point on the $V$-$P$ plane at which both the numerator and the denominator of the equation are zero separately is a singular point. The singular points should be on the curve given by the following set of equations.

$$V + \frac{\alpha}{2A\sqrt{P_s}}P - \alpha\sqrt{P_s}\frac{\rho}{2A} = 0 \quad \cdots\cdots(30)$$

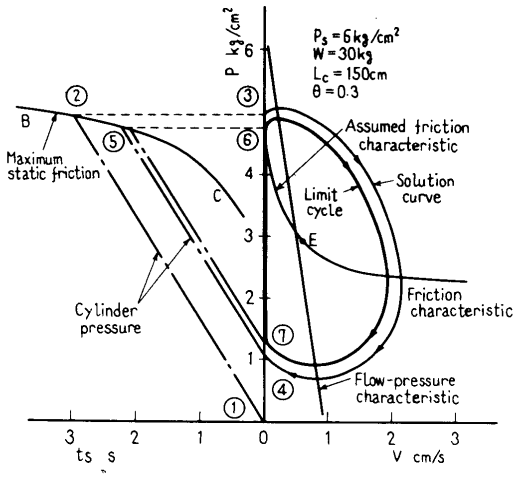


Fig.10 Solution curve by graphical method ($\theta = 0.3$)

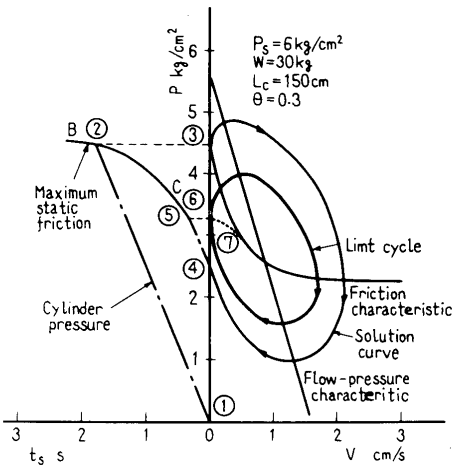


Fig.11 Solution curve by graphical method ($\theta = 0.5$)

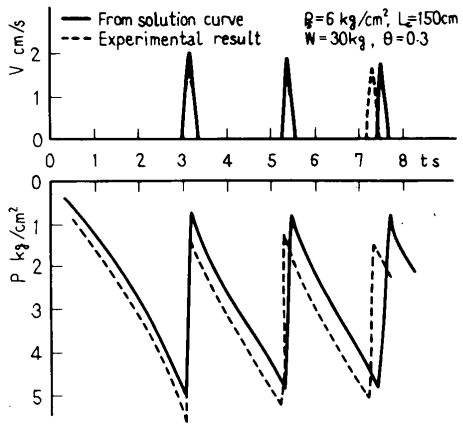


Fig.12(a) Wave forms of $V$ and $P(\theta = 0.3)$

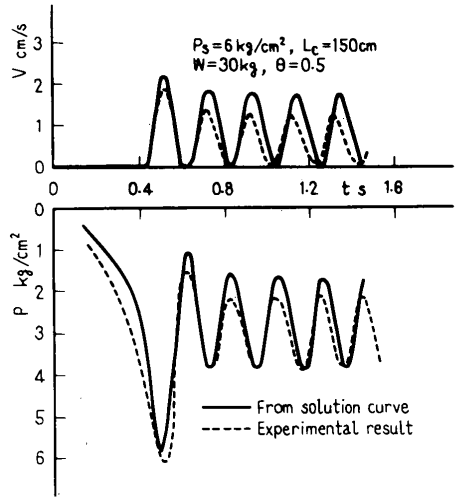


Fig.12(b) Wave forms of $V$ and $P(\theta = 0.5)$

$$P - \frac{1}{A}\{ f(V) + FV \} = 0 \quad \cdots\cdots\cdots(31)$$

If the singular point is stable, the trajectory converges to this point. However, if it is unstable, the trajectory moves away from it and should approach some limit cycle. To see if a point is stable we write Eq.(19) in the following form, expanding the nonlinear terms and retaining only the first order terms.

$$\frac{dp}{dv} = \frac{av + bp}{cv + dp} \quad \cdots\cdots\cdots\cdots\cdots(32)$$

Here, $a$, $b$, $c$ and $d$ are as follows.

$$\left.\begin{aligned} a &= -(2A)/(\beta G) \\ b &= -\alpha(\theta)/(\beta G\sqrt{P_S}) \\ c &= -\{ f'(V) + F \}/M \\ d &= A/M \end{aligned}\right\} \quad \cdots\cdots\cdots(33)$$

It is known that the stability of a singular point is determined by studying the set of parameters by Table 1.[18][19] The boundaries of the regions of the various states in Table 1 are obtained as shown in Fig.13 or 14, by taking different sets of quantities as an ordinate and an abscissa. For example from Fig.13, it is seen that the system will tend to vibrate when the friction characteristic $df/dV$ is small and the value of flow rate is also small. From Fig.14, it is seen that the system will tend to vibrate when $M$ is small.

Four points, $A'$, $B'$, $C'$ and $D'$ indicated in Figs.13 and 14, correspond to the singular points shown in Fig.6. It is seen that the criterion obviously gives the correct classification of the points in experiments also.

## 4. Discussion

### 4.1 Flow-pressure characteristics

The relation between $dX/dt$ and the pressure $P$ is given by Eq.(11).

Table 1 Coefficients of characteristic equation

| | | |
|---|---|---|
| I | $(b-c)^2 + 4ad > 0$<br>(A) $ad - bc < 0$<br>Nodal point | $b + c < 0$ Stable<br>$b + c > 0$ Unstable |
| | (B) $ad - bc > 0$<br>Saddle point | |
| II | $(b-c)^2 + 4ad < 0$<br>(A) $b + c = 0$<br>Center | |
| | (B) $b + c \neq 0$<br>Spiral point | $b + c < 0$ Stable<br>$b + c > 0$ Unstable |
| III | $(b-c)^2 + 4ad = 0$<br>Nodal point | $b + c < 0$ Stable<br>$b + c > 0$ Unstable |

$$2A\frac{dX}{dt} + \beta G\frac{dP}{dt} = \alpha(\theta)\sqrt{P_S}\left(\rho - \frac{P}{P_S}\right)$$

When the piston moves smoothly without vibration, $dP/dt=0$. Then, writing $dX/dt = V$, we have the following relation

$$P = -\left(\frac{2A\sqrt{P_S}}{\alpha(\theta)}\right)V + \rho P_S$$

This is a straight line that crosses the $P$-axis at $\rho P_S$ with a gradient of $-2A\sqrt{P_S}/\alpha(\theta)$. Within the range of this experiment, the flow-pressure characteristic does indicate the linearity. Therefore, Eq.(11) can be a quite satisfactory approximation of the real flow-pressure characteristic. Physically, the characteristic curve should cross the $P$-axis at $P_S$, be-

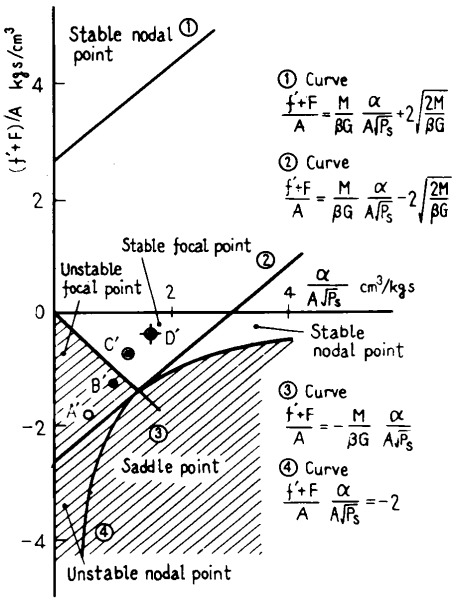


Fig.13 Stable region in $\alpha/(A\sqrt{P_S}) - (f'+F)/A$ plane

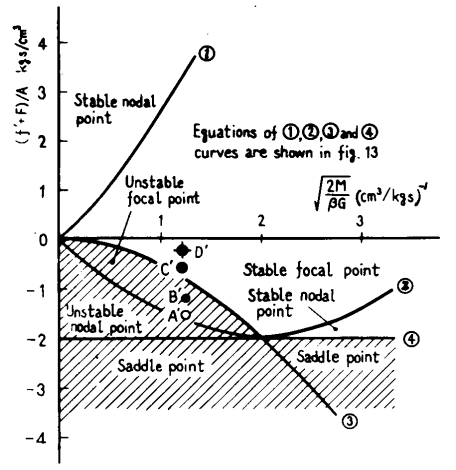


Fig.14 Stable region in $\sqrt{2M/\beta G} - (f' + F)/A$ plane

cause then the system is completely staying still. However, because the equation is approximate, it crosses the $P$-axis at $\rho P_S$.

4.2 Values of parameters in the experiment

In comparing the result of experiments with the theoretical analysis, the following values of parameters were used,

$M_0$ : $W = M_0 g$ varied from 20kg to 100kg

$L_c$ : Length of conduit = 150cm

$A_c$ : Effective area of cylinder = $10cm^2$

$G_0$ : Volume of cylinder = $125cm^3$

$G = G_0 + A_c L_c = 200cm^3$

$\beta$ : As the modulus of compressibility can not be easily measured, $\beta = 0.0007 - 0.001 cm^2/kg$ is assumed.

The demonstrated figures of trajectory and wave forms are just two examples of vibratory motions. The values of $m$, the magnifying factor of $V$-axis for the application of Li'enard's method, were between 1.0 and 1.2 in most examples.

## 5. Conclusions

Experiments were conducted on a hydraulic drive system with a relatively low slide friction for the vibratory motion of the piston under various loads and other conditions. It was found that both the stick-slip motion and motion without sticking took place in low speed operation. By setting up the nonlinear equations of motion and flow-pressure characteristic, the analysis was made of the motion considering also the time dependency of the maximum static friction. The use of a graphical method to obtain limit cycles and a stability analysis to find the stability region was quite effective in making clear the mechanism with which the motion took place. The comparison of the result of experiment with the result of analysis by the equations of motion, revealed a striking agreement of the two results even in the wave forms of $P$ and $V$ with respect to time.

A more exact estimation of the value of $\beta$ and the shape of the friction characteristic in the region near zero velocity is probably the subject for further study.

## References


(1) Makino,S., et al., Journal of Mechanical Laboratory(in Japanese), Vol.10, No.6(1956), p.237 Vol.11, No.3(1957), p.95.

(2) Matsuzaki,J. and Hashimoto,S., Trans. Japan Soc. Mech. Engrs.(in Japanese), Vol.28, No.194(1962),p.1394.

(3) Matsuzaki,J., Trans. Japan Soc. Mech. Engrs.(in Japanese), Vol.29, No.206 (1963), p.977.

(4) Okamura,K., et al., Jour. Japan Soc. Prec. Engrs. (in Japanese), Vol.34, No.11(1968), p.731.

(5) Okamura,K., et al., Jour. Japan Soc. Prec. Engrs. (in Japanese), Vol.34, No.12(1968), p.774.

(6) Okamura,K. and Matsubara,T., Jour. Japan Soc. Prec. Engrs. (in Japanese), Vol.35, No.9(1969), p.561.

(7) Okamura,K., et al., Jour. Japan Soc. Prec. Engrs. ( in Japanese ), Vol.35, No.8(1969), p.490.

(8) Muto,T. and Hattori,T., Trans. Japan Soc. Mech. Engrs. (in Japanese), Vol. 39, No.328(1973),p.3740.

(9) Kato,S. and Matsubayashi,T., Trans. Japan Soc. Mech. Engrs.(in Japanese), Vol.35, No.273(1969), p.1138.

(10) Kato,S., et al., Trans. Japan Soc. Mech. Engrs.(in Japanese), Vol.35, No. 273(1969), p.1147.

(11) Singh,B.R., Trans. ASME, Ser. A, No.59 (1959), p.146. Ser. B, No.82(4)(1960), p.393.

(12) Hunt,J.B., et al., Wear, Vol.8(1965), p.455.

(13) Bell,R. and Burdekin,M., Proc. Inst. Mech. Engrs., Vol.184, pt.1, No.30 (1969-70), p.543,560.

(14) Rowson,D.M., Wear, Vol.31(1975), p. 213.

(15) Antonion,S.S., et al., Wear, Vol. 36 (1976), p.235.

(16) Nakagawa,T. and Takase,H., Bull. Fac. Engng. Toyama Univ.(in Japanese),Vol. 23, No.1-2(1972), p.73.

(17) Ikebe,H., et al., Servo Mechanism and Element(in Japanese)(1973), p.240-250 OHM

(18) Stoker,J.J., Nonlinear Vibration in Mechanical and Electrical System (1950), Inter Science Publishers.

(19) Sawaragi,Y., Nonlinear Vibration (1965), Kyoritsu Publishers, p.36.